Photon-Phonon-Enhanced Infrared Rectification in a Two-Dimensional Nanoantenna-Coupled Tunnel Diode

Emil A. Kadlec, Robert L. Jarecki, Andrew Starbuck, David W. Peters, and Paul S. Davids*

Sandia National Laboratories, Albuquerque, New Mexico 87185, USA

(Received 11 September 2016; revised manuscript received 17 November 2016; published 28 December 2016)

The interplay of strong infrared photon-phonon coupling with electromagnetic confinement in nanoscale devices is demonstrated to have a large impact on ultrafast photon-assisted tunneling in metal-oxide-semiconductor (MOS) structures. Infrared active optical phonon modes in polar oxides lead to strong dispersion and enhanced electric fields at material interfaces. We find that the infrared dispersion of SiO_2 near a longitudinal optical phonon mode can effectively impedance match a photonic surface mode into a nanoscale tunnel gap that results in large transverse-field confinement. An integrated 2D nanoantenna structure on a distributed large-area MOS tunnel-diode rectifier is designed and built to resonantly excite infrared surface modes and is shown to efficiently channel infrared radiation into nanometer-scale gaps in these MOS devices. This enhanced-gap transverse-electric field is converted to a rectified tunneling displacement current resulting in a dc photocurrent. We examine the angular and polarization-dependent spectral photocurrent response of these 2D nanoantenna-coupled tunnel diodes in the photon-enhanced tunneling spectral region. Our 2D nanoantenna-coupled infrared tunnel-diode rectifier promises to impact large-area thermal energy harvesting and infrared direct detectors.

DOI: 10.1103/PhysRevApplied.6.064019

I. INTRODUCTION

Quantum and thermal fluctuations give rise to radiative energy transfer between vacuum-separated finite-temperature objects [1–7]. These fluctuation-induced light-matter interactions can be the source for radiative thermoelectric conversion in nanostructured systems. Photon-phonon–enhanced tunneling is a quantum thermal process in which nanoscale-confined transverse electromagnetic fields [8] combine with infrared phonon resonances to enhance the tunneling photoresponse [9]. By designing plasmonic or photonic surface-mode resonances to spectrally overlap phonon modes in polar oxide materials, a large photoresponse has been shown to occur due to the strong coupling of infrared radiation into nanoscale tunnel barriers leading to tunneling rectification [9,10]. The direct conversion of infrared radiation to electrical current through rectification has been the subject of research over the years [11–14] due to the potential for direct heat to electrical energy conversion.

Previously, we reported direct infrared rectification in a large-area 1D gratinglike nanoantenna-coupled metal-oxide-semiconductor (MOS) tunnel diode [9]. Resonant enhancement of transverse fields in the tunnel barrier is observed in the region near the longitudinal optical (LO) phonon mode in silicon dioxide. By matching the nanoantenna transverse-magnetic (TM) spoof surface-mode grating resonance [15,16] to the epsilon-near-unity region of the oxide dispersion, we observe large transverse-field confinement in the tunnel oxide that leads to an enhanced polarized TM photocurrent for our room-temperature 1D rectenna. In this paper, we examine the polarization response and field-enhancement performance of a 2D cross-dipole nanoantenna-coupled MOS tunnel diode. The polarized absorbance as a function of the angle and wavelength are measured and compared to simulated results. Transverse-field enhancement is predicted in the region near the oxide LO phonon resonance with maximum field concentration when the real part of the oxide permittivity equals unity. Qualitatively, the photonic modes in the 2D cross-dipole structure are discussed and seen to arise from strong coupling of material dispersion and surface-diffracted mode resonances. Experimental photocurrent angular spectral maps show an enhanced photocurrent in this region near the surface-mode dispersion. Thermal effects that arise due to the oxide absorption are discussed.

II. MODEL AND EXPERIMENT

The nanoantenna pattern under consideration is a cross-dipole frequency-selective surface that is known to possess excellent absorption characteristics in the infrared and to exhibit polarization-insensitive absorption in an angular range around normal incidence. Figure 1(a) shows the cross-dipole unit cell and (b) shows the SEM cross section of the cross-dipole nanoantenna-coupled tunnel diode. The inset shows a high-resolution TEM of the device cross

*pdavids@sandia.gov

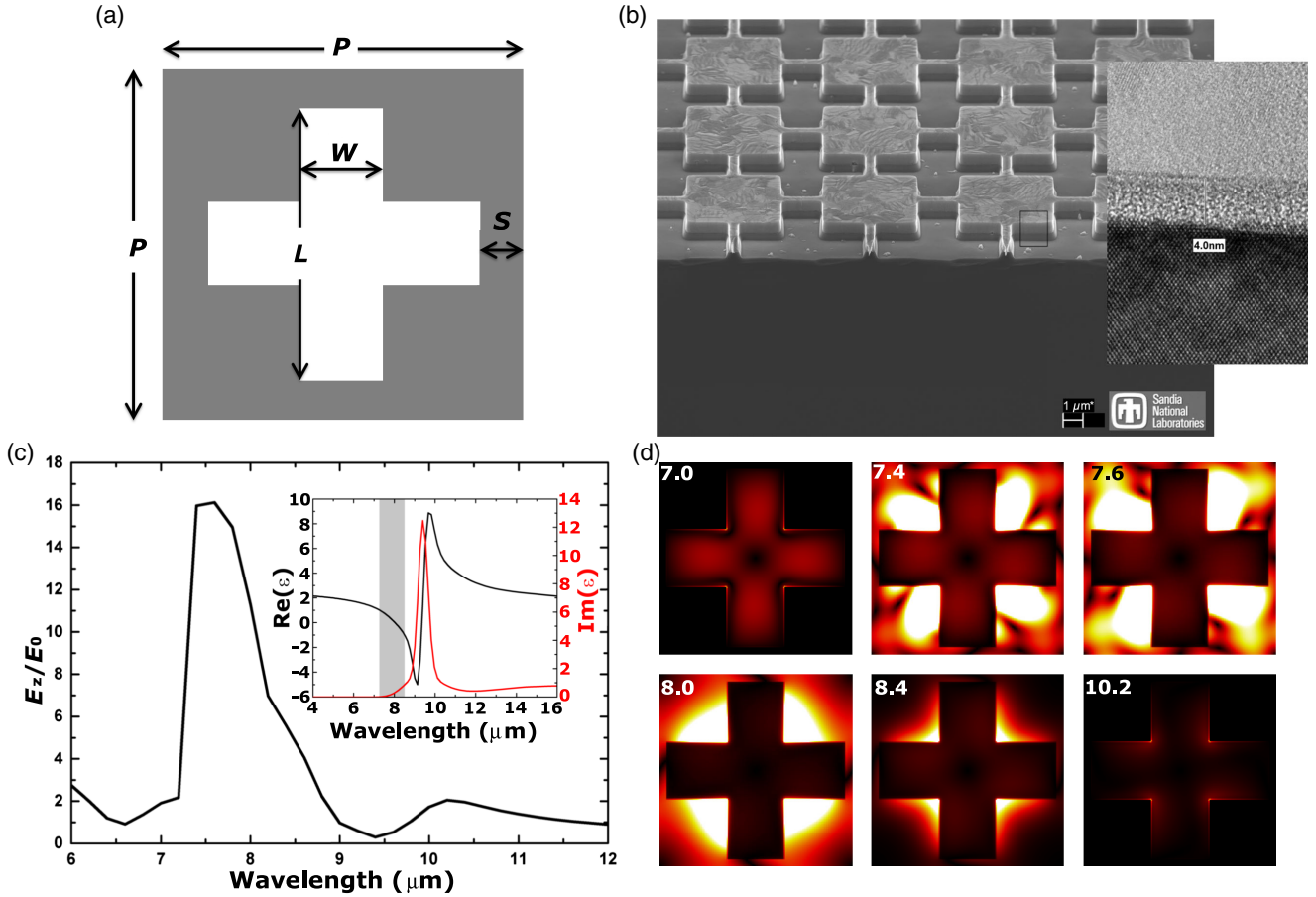

FIG. 1. Illustration of a large-area 2D nanoantenna-coupled n-type MOS tunnel diode with a field-concentration mechanism. (a) The schematic shows the unit-cell pattern for the cross-dipole antenna-coupled diode. Here P is the unit-cell period, w is the width, and L is the length of the 2D cross. (b) A SEM micrograph of the 2D array before HDP oxide overcladding and chemical mechanical polish steps. The inset is a high-resolution TEM of the MOS tunnel diode. The oxide tunnel gap is measured to be 4 nm across. (c) Electromagnetic simulations of the E_z transverse-field confinement in the oxide tunnel barrier as a function of the incident wavelength. The inset shows measured values of the complex permitivity for HDP-deposited oxide. The gray band indicates $-1 < \mathrm{Re}(\epsilon) \leq 1$ signifying the enhanced tunneling region. (d) E_z field slices on the x-y plane in the tunnel barrier oxide for select wavelengths.

section illustrating the 4-nm tunnel-oxide gap separating the 700-nm-thick Al antenna from the heavily doped n^+ Si ground plane [17], which acts as both a reflective surface in the infrared and as an electrical contact. It is important to note that the metal nanoantenna pattern in Fig. 1(b) is backfilled with high-density-plasma (HDP) oxide and planarized leaving 200 nm oxide covering the metallic structure. The fabrication process is the same as for the 1D nanoantenna and described in detail in Ref. [9]. Here, $P = 6.0$ μm is the period of the antenna array, $w = 1.2$ μm is the aperture opening width, and $L = 5.5$ μm is the dipole length. The simulated transverse field in the oxide tunnel barrier is shown for right-handed circularly polarized light incident on the 2D periodic array. The field enhancement in the oxide tunnel gap for the cross dipole is shown in the gray band in the inset in Fig. 1(c), with Fig. 1(d) denoting the E_z field profiles. A large E_z field enhancement, $16.6\sqrt{2} \simeq 24\times$ in linear polarization, is seen as the real part of the permittivity of the oxide approaches unity. This impedance-matching condition at $\mathrm{Re}(\epsilon) = 1$ gives rise to perfect coupling to the photonic surface resonance and maximal transverse field in the tunnel gap [18]. The photonic surface mode induces a surface current on the metal patch that acts to launch a transverse electromagnetic mode into the metal-insulator gap, thus creating the large edge peaked E_z field concentration under the metal at the impedance-matching condition. As the permittivity decreases, the E_z field enhancement decreases, going to zero at the transverse-optical (TO) phonon resonance wavelength of 9.4 μm. This corresponds to the peak absorption in oxide. The inset in Fig. 1(c) shows the measured HDP oxide complex permittivity. The gray region corresponds to the wavelength band where $-1 < \mathrm{Re}(\epsilon) \leq 1$.

A. Infrared reflectance spectrum

The infrared absorption spectra of the 2D cross-dipole pattern can be obtained as a function of the angle and polarization using a hemispherical directional reflectometer

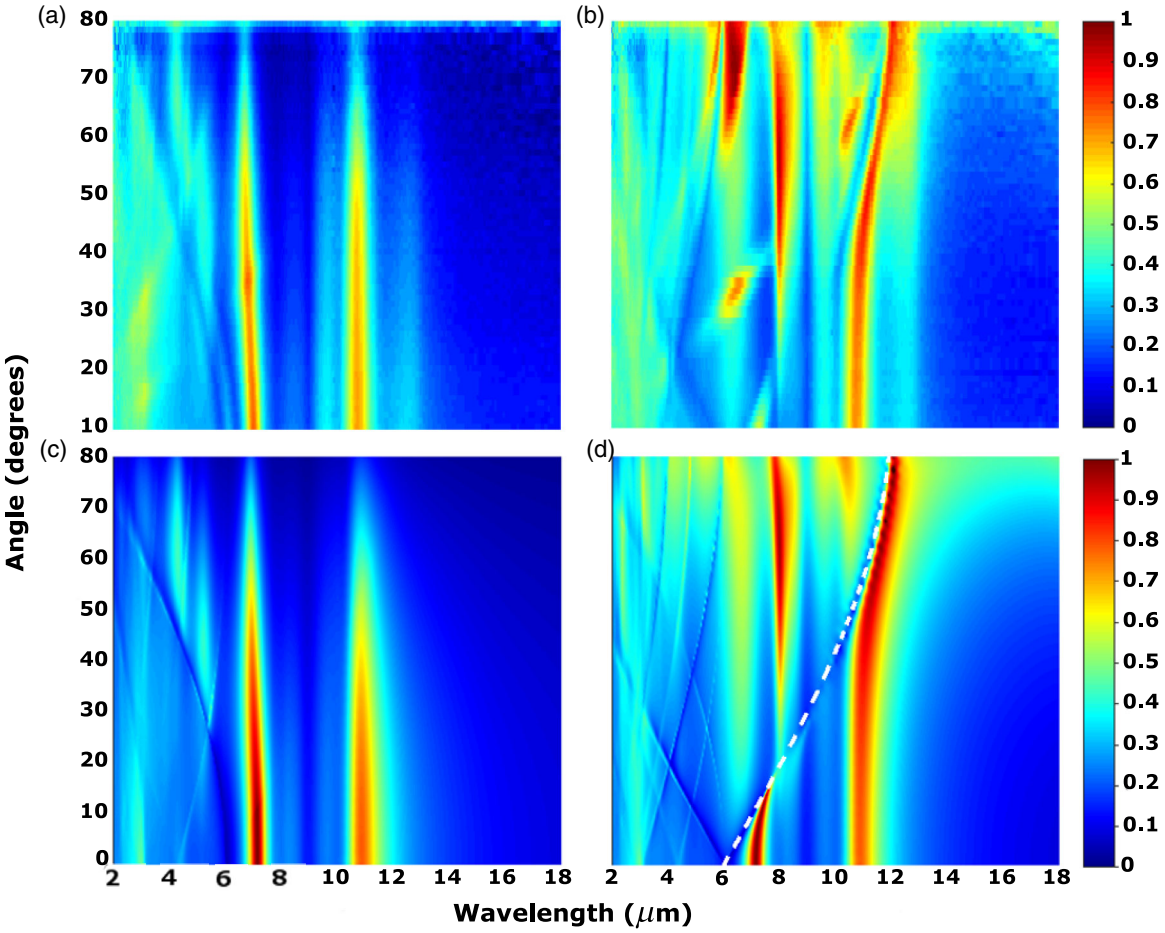

FIG. 2. Polarized angular absorption spectra for large-area 2D cross-dipole antenna-coupled tunnel diodes. (a) Measured TE absorption. (b) Measured TM absorption. (c) RCWA-modeled TE absorption and (d) modeled TM absorption. The dashed line indicates the $n = +1$ surface-diffracted mode. The antenna cross-dipole parameters are $P = 6$ μm, $w = 1.2$ μm, and $L = 5.5$ μm. The fabricated device area is 4 mm $\times$ 4 mm.

(HDR). Figure 2 shows a comparison of the measured TE- and TM-polarized angular absorption spectrum to the simulated rigorous coupled-wave analysis (RCWA) computed spectra. The RCWA-computed and HDR-measured angular spectra are seen to be in excellent agreement. The experimental angular spectra begins at 10° off-normal incidence due to limitations of the HDR, and the simulated spectra begin at normal incidence. The angular spectra show absorption features resulting from a combination of thin-film resonances and structural photonic resonances from the underlying 2D periodic pattern. Figure 2(d) shows the computed TM angular absorption spectra with a diffracted surface-mode dispersion shown as a white dashed line. A diffraction analysis of the 2D periodic cross-dipole nanoantenna gives

$$k[\sin(\theta_i) + \sin(\theta_r^n)] = \frac{2\pi}{P} n, \qquad (1)$$

where $n = 0, \pm 1, \pm 2, \ldots$ and $k = 2\pi/\lambda$ with λ the incident wavelength. This surface diffraction mode exists for $n = +1$, such that $\sin(\theta_r^{+1}) = 1$, and the dispersion curve is $\theta_i = \sin^{-1}(\lambda/P - 1)$. The surface-mode dispersion is between wavelength limits $P \leq \lambda < 2P$. Furthermore, it sets the upper limit for the angular range of the enhanced transverse-field coupling and polarization independence, which for our device parameters is roughly 18° from normal incidence. The 2D cross-dipole absorption spectra show resonant TE and TM incident infrared radiation is strongly absorbed. The complex modes in these 2D photonic structures lead to transverse-field confinement and an improved photoresponse through the interaction of periodic structural modes and the dispersive material resonances.

B. Modal description

In order to understand the complex composite modes of the 2D antenna-coupled diode, we break the complete 2D cross-dipole structure down into its base components. The base components consist of a series of thin-film structures and patterned structures without the oxide fill and overcoat. The actual measured device features a 200-nm overetch

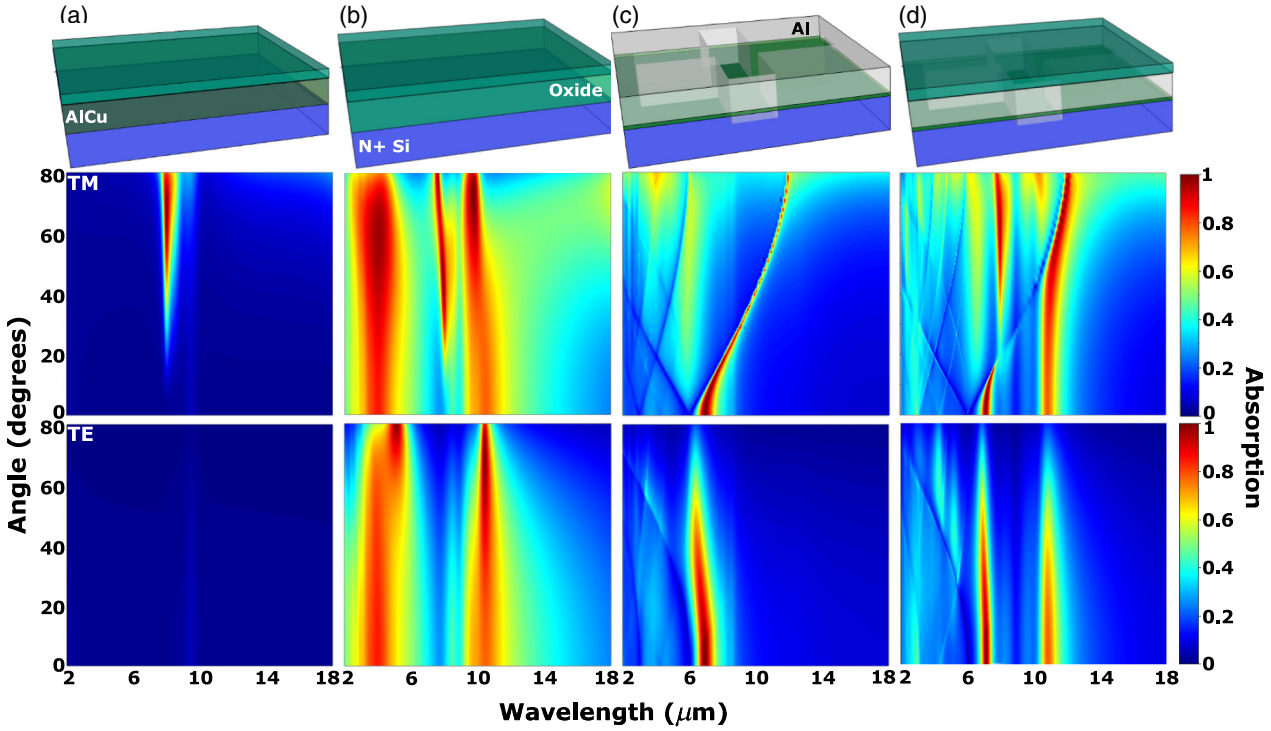

FIG. 3. Evolution of modes in the composite 2D rectenna structure. Schematic of the rectenna composite with simulated TE and TM absorption. EM radiation is incident to the top surface (surface opposite of the n^+ Si substrate). (a) Computed absorption in 200 nm oxide film on top of an AlCu metal film. (b) Thick 1.1 μm oxide on a heavily doped n^+ Si substrate. (c) Patterned 2D rectenna cross dipole without oxide fill. (d) Full 2D rectenna cross dipole with oxide backfill including a 200-nm oxide overcoat of the entire structure. This is the actual fabricated structure including an overetch of 200 nm into the n^+ Si layer.

into the n^+ substrate and is backfilled with oxide and overclad with 200 nm of oxide above the metal [see Fig. 3(d)]. Figures 3(a)–3(d) show the series of base components under consideration. Figure 3(a) represents a thin dispersive oxide film (200 nm thick) on a planar AlCu metal film. The TM absorption feature at large angles ($\geq 45°$) of incidence occurs at the LO phonon wavelength of $\lambda_{LO} = 8.1$ μm. This is the well-known Berreman mode [19] or epsilon-near-zero (ENZ) mode in the dispersive oxide thin film on a metal. The second base component shown in Fig. 3(b) is a thick oxide (1.1 μm) on a heavily doped n^+ silicon substrate. The thick oxide on n^+ Si angular absorption spectra shows both broad TE and TM absorption at 10.8 μm for most angles of incidence. The large absorption feature at 4.0 μm represents the plasma wavelength of the n^+ silicon which marks the boundary between metalliclike opacity and transparency. It is important to note that the Berreman mode is still present in the thick oxide film on the n^+ Si substrate. Figure 3(c) represents the structural photonic modes that exist due to the patterned metallic 2D cross-dipole periodic structure. The TM and TE structural modes are designed to have high absorption in the epsilon-near-unity spectral region to give maximal transverse-field enhancement and confinement in the oxide-filled tunnel barrier. The angular range of the TM absorption for the photonic structural mode is clearly limited by the surface-diffracted mode dispersion. In the region below the surface-mode dispersion line, both the TE and TM modes exist at roughly 7.2 μm. In the angular range above the surface-mode dispersion line, only the TE mode exists, and it bends toward a shorter wavelength with an increasing angle of incidence. Figure 3(d) shows the mode structure for the complete oxide-filled and overclad 2D cross-dipole antenna-coupled diode that was fabricated and measured. The Berreman or ENZ mode in the complete overclad structure is seen at high angles of incidence for TM polarization as are the thin-film TE and TM oxide modes for the thick oxide on the n^+ Si substrate. These oxide modes at 10.8 μm are narrower than the modes seen in the bulk thin-film case. Furthermore, they occur in a region where the oxide behaves as a lossy dielectric and give rise to high oxide absorption in the filled overclad structure. The photonic surface-diffracted modes are designed to spectrally overlap the oxide material dispersion in the epsilon-near-unity region for maximal enhanced transverse-field confinement in the tunnel oxide barrier. These surface-diffracted modes are basically a function of the periodic nature of the structure. While this examination of the thin film and photonic modes is not a rigorous modal decomposition, it does provide qualitative insight into the various absorption processes and is a useful design guideline.

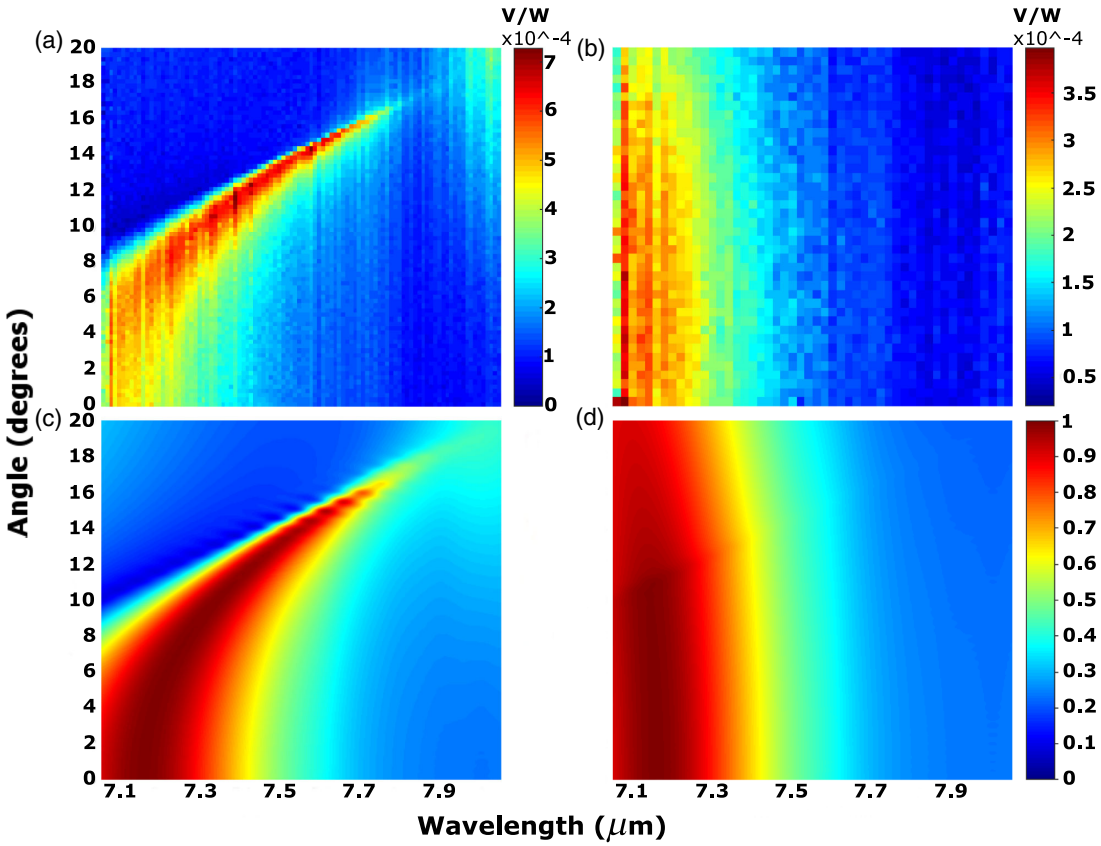

FIG. 4. Photocurrent maps of the 2D rectenna cross-dipole structure using direct scanned quantum cascade laser (QCL) illumination. Polarized photocurrent maps and simulated absorption of a large-area 2D cross-dipole nanoantenna-coupled tunnel-diode rectifier at zero bias. (a) TM-polarized photocurrent measurements. (b) TE-polarized photocurrent measurements. (c) TM-simulated absorption spectrum. (d) TE-simulated absorption spectrum. All measured photocurrent spectra are normalized to the input power and are given in V/W units.

C. Photocurrent map

So far, we have examined the electromagnetic response of the 2D cross-dipole coupled tunnel diode only. The impact of the enhanced transverse-field confinement can be seen in the measured photocurrent of the nanoantenna-coupled tunnel diode. The angular photocurrent spectrum is measured using a tunable QCL laser with a wavelength tuning range from 7 to 11 μm. The sample under test is mounted on a rotation stage, and the polarization of the laser output is controlled by a polarizer in the beam path. The beam size of 2-mm diameter underfills the large area of the nanoantenna-coupled diode. As we vary the angle of incidence, the beam becomes elliptical and the illuminated area increases slightly. Figure 4 shows the measured zero-bias angular photocurrent spectrum for TE- and TM-polarized light in the tunneling-enhanced region. The TM photocurrent is seen to be enhanced for oblique incidence near the surface-mode dispersion limit in the region near unit permittivity. The TE-mode photocurrent does not show a peak for oblique incidence and has a nearly uniform photocurrent over the measured angular range. The enhanced photocurrent in the epsilon-near-unity region is where the simulation predicts tunneling rectification to take place due to the large transverse-field confinement in the tunnel oxide. The computed RCWA absorption is shown for comparison in Fig. 4, where the measured photocurrent closely follows the photonic structural absorption. The oxide optical absorption from the measured n and k in the enhanced tunneling region is small ($10^{-2}\mu\mathrm{m}^{-1}$) but increases monotonically, reaching a maximum ($3.1\ \mu\mathrm{m}^{-1}$) at the TO phonon resonance at 9.3 μm.

Oxide absorption modes at 10.8 μm seen in the back-filled structure in Fig. 3 can lead to absorptive heating of the structure under QCL or blackbody illumination. A recent examination of infrared metal-insulator-metal rectenna structures leads to the conclusion that tunneling rectification may just be a Seebeck-induced potential drop across metal-insulator-metal contacts [20]. In our 2D cross-dipole rectenna, nonuniform absorption in the antenna-coupled tunnel diode could lead to temperature gradients that induce a voltage drop across the tunnel diode. This nonuniform absorption thermal effect is amplified by the large Seebeck coefficient of doped Si. The Seebeck coefficient of n-doped Si [21], $S_{n\text{-Si}} = -0.4$ mV/K, is orders of magnitude larger than for metals, $S_{\mathrm{Al}} = 3.5\ \mu\mathrm{V/K}$. An experimental signature of a thermally

induced voltage difference across the tunnel junction is a photovoltaic shift in the current minimum under illumination. This shift is not seen in the illuminated *IV*'s, so either the nonuniform induced temperature difference is small or the absorption-induced Seebeck effect is weak. Engineering the nonuniform absorption Seebeck effect in the 3D rectenna structure could potentially be very beneficial in effectively self-biasing the tunnel rectifier, improving the conversion of radiated heat into electrical power.

Uniform heating of the 2D cross-dipole rectenna resulting from the absorption of the structure could lead to bolometric effects in the device, where temperature-dependent resistance changes would be observed. The choice of a direct tunneling diode rather than a Schottky or other semiconductor diode is in part to limit the effect of temperature on the *IV* current-voltage characteristics. Tunneling diodes are very weakly temperature dependent and, when operated unbiased, are expected to give a negligible open-circuit current. To experimentally observe the fast tunneling versus the slow thermal time constant, we could measure the temporal photoresponse of our device. Unfortunately, our large-area MOS devices have very large capacitances such that the *RC* time constant of the device limits the temporal response to below thermal time scales. This type of temporal approach is possible with small-area-scaled devices and will be the subject of further work.

III. CONCLUSIONS

In summary, it is shown that, by using the oxide infrared dispersion near a LO phonon resonance, we can impedance match into a 2D surface-diffracted mode photonic resonance which gives rise to high transverse-field confinement in a nanometer-scale gap. The gap-confined transverse field acts as an ultrafast displacement current in the MOS tunnel diode that interacts with the diode *IV* nonlinearity, resulting in an enhanced tunneling-rectified photoresponse. This can be compared to the previously studied 1D gratinglike antenna-coupled diode [9], where the incoming light excites a TM spoof-plasmon ENZ resonance that is impedance matched into the gap mode. A compositional modal picture of the complete oxide overclad device is developed and shows that thin-film modes persist and interact with the surface-diffracted modes resulting from the periodic 2D patterning. A strong infrared photoresponse for both TE and TM illumination of the unbiased device is seen in the spectral region near $0 < \mathrm{Re}(\epsilon) \leq 1$ and in the angular range below the surface-diffracted mode dispersion.

Metal-oxide-semiconductor-based tunneling rectifiers allow for the optimization of the infrared photoresponse through doping, band alignment, and work-function variation by utilizing alternative metals and infrared-active polar dielectrics. Furthermore, radiometric measurement of optimized devices using real graybody thermal sources will be developed and used to assess the viability of this radiative thermoelectric conversion method.

ACKNOWLEDGMENTS

Funding for this work was provided by Sandia's Laboratory Directed Research and Development (LDRD) program. Sandia is a multimission laboratory operated by Sandia Corporation, a Lockheed Martin Company, for the United States Department of Energy's National Nuclear Security Administration under Contract No. DE-AC04-94AL85000.

[1] S.-A. Biehs, Emmanuel Rousseau, and J.-J. Greffet, Mesoscopic Description of Radiative Heat Transfer at the Nanoscale, Phys. Rev. Lett. **105**, 234301 (2010).

[2] S.-A. Biehs, Felipe S. S. Rosa, and Philippe Ben-Abdallah, Modulation of near-field heat transfer between two gratings, Appl. Phys. Lett. **98**, 243102 (2011).

[3] J. J. Loomis and H. J. Maris, Theory of heat transfer by evanescent electromagnetic waves, Phys. Rev. B **50**, 18517 (1994).

[4] Arvind Narayanaswamy, Sheng Shen, Lu Hu, Xiaoyuan Chen, and Gang Chen, Breakdown of the Planck blackbody radiation law at nanoscale gaps, Appl. Phys. A **96**, 357 (2009).

[5] R. Ottens, V. Quetschke, Stacy Wise, A. Alemi, R. Lundock, G. Mueller, D. Reitze, D. Tanner, and B. Whiting, Near-Field Radiative Heat Transfer between Macroscopic Planar Surfaces, Phys. Rev. Lett. **107**, 014301 (2011).

[6] Bai Song, Dakotah Thompson, Anthony Fiorino, Yashar Ganjeh, Pramod Reddy, and Edgar Meyhofer, Radiative heat conductances between dielectric and metallic parallel plates with nanoscale gaps, Nat. Nanotechnol. **11**, 509 (2015).

[7] Raphael St-Gelais, Linxiao Zhu, Shanhui Fan, and Michal Lipson, Near-field radiative heat transfer between parallel structures in the deep subwavelength regime, Nat. Nanotechnol. **11**, 515 (2015).

[8] P. K. Tien and J. P. Gordon, Multiphoton Process Observed in the Interaction of Microwave Fields with the Tunneling between Superconductor Films, Phys. Rev. **129**, 647 (1963).

[9] Paul S. Davids, Robert L. Jarecki, Andrew Starbuck, D. Bruce Burckel, Emil A. Kadlec, Troy Ribaudo, Eric A. Shaner, and David W. Peters, Infrared rectification in a nanoantenna-coupled metal-oxide-semiconductor tunnel diode, Nat. Nanotechnol. **10**, 1033 (2015).

[10] Pai-Yen Chen, Mehdi Hajizadegan, Maryam Sakhdari, and Andrea Alù, Giant Photoresponsivity of Midinfrared Hyperbolic Metamaterials in the Photon-Assisted-Tunneling Regime, Phys. Rev. Applied **5**, 041001 (2016).

[11] A. Sanchez, S. K. Singh, and A. Javan, Generation of infrared radiation in a metal-to-metal point-contact diode at synthesized frequencies of incident fields: A high-speed broad-band light modulator, Appl. Phys. Lett. **21**, 240 (1972).

[12] A. Sanchez, C. F. Davis, K. C. Liu, and A. Javan, The MOM tunneling diode: Theoretical estimate of its performance at microwave and infrared frequencies, J. Appl. Phys. **49**, 5270 (1978).

[13] Sachit Grover, Olga Dmitriyeva, Michael J. Estes, and Garret Moddel, Traveling-wave metal/insulator/metal diodes for improved infrared bandwidth and efficiency of antenna-coupled rectifiers, IEEE Trans. Nanotechnol. **9**, 716 (2010).

[14] Steven J. Byrnes, Romain Blanchard, and Federico Capasso, Harvesting renewable energy from Earth's mid-infrared emissions, Proc. Natl. Acad. Sci. U.S.A. **111**, 3927 (2014).

[15] F. J. Garcia-Vidal, L. Martín-Moreno, and J. B. Pendry, Surfaces with holes in them: New plasmonic metamaterials, J. Opt. A **7**, S97 (2005).

[16] P. S. Davids, F. Intravaia, and D. A. R. Dalvit, Spoof polariton enhanced modal density of states in planar nanostructured metallic cavities, Opt. Express **22**, 12424 (2014).

[17] James C. Ginn, Robert L. Jarecki, Eric A. Shaner, and Paul S. Davids, Infrared plasmons on heavily-doped silicon, J. Appl. Phys. **110**, 043110 (2011).

[18] R. D. Kekatpure and P. S. Davids, Channeling light into quantum-scale gaps, Phys. Rev. B **83**, 075408 (2011).

[19] D. W. Berreman, Infrared absorption at longitudinal optic frequency in cubic crystal films, Phys. Rev. **130**, 2193 (1963).

[20] M. Bareiß, P. M. Krenz, G. P. Szakmany, B. N. Tiwari, D. Kälblein, A. O. Orlov, G. H. Bernstein, G. Scarpa, B. Fabel, U. Zschieschang, H. Klauk, W. Porod, and P. Lugli, Rectennas revisited, IEEE Trans. Nanotechnol. **12**, 1144 (2013).

[21] T. H. Geballe and G. W. Hull, Seebeck effect in silicon, Phys. Rev. **98**, 940 (1955).